



Width evolution of channel belts as a random walk

Jens M. Turowski^{1,2}, Fergus M^cNab¹, Aaron Bufe^{1,3}, Stefanie Tofelde⁴

¹ Helmholtz Zentrum Potsdam, GeoForschungsZentrum (GFZ) Potsdam, Potsdam, Germany

² State Key Laboratory of Hydrosience and Engineering, Tsinghua University, Beijing, China

5 ³ Department of Earth and Environmental Sciences, Ludwig Maximilian University Munich, Munich, Germany

⁴ Institute of Geological Sciences, Freie Universität Berlin, Berlin, Germany

Correspondence to: Jens M. Turowski (jens.turowski@gfz-potsdam.de)

Abstract. Channel belts, floodplains and fluvial valley floors form by the mobilization and deposition of sediments during the lateral migration of rivers. Channel-belt width and its temporal evolution is important for the hydraulics, hydrology, and ecology of floodplains, and for human activities such as farming, protecting infrastructure, and natural hazard mitigation. Yet, we currently lack a comprehensive theoretical description of the width evolution of channel belts. Here, we explore the predictions of a physics-based model of channel-belt width for the transient evolution of channel belts. The model builds on the assumption that the switch of direction of a laterally migrating channel can be described by a Poisson process, with a constant rate parameter related to channel hydraulics. As such, the lateral migration of the channel can be viewed as a non-standard one-dimensional random walk. The model predicts three phases in the growth of channel belts. First, before the channel switches direction for the first time, the channel belt grows linearly. Second, as long as the current width is smaller than the steady state width, growth follows an exponential curve on average. Finally, there is a drift phase, in which the channel-belt width grows with the square root of time. We exploit the properties of random walks to obtain equations for the distance from a channel that is unlikely to be inundated in a given time interval (law of the iterated logarithm), distributions of first passage time and return to the origin, and the mean lateral drift speed of steady state channel belts. All of the equations can be directly framed in terms of the channel's hydraulic properties, in particular its lateral transport capacity that quantifies the amount of material that the river can move in lateral migration per unit time and channel length. Finally, we derive the distribution of sediment residence times, and show that its right-hand tail follows a power-law scaling with an exponent of -1.5. As such, the mean and variance of ages of sediment deposits in the channel belt do not converge to stable values, but depend on the time since the formation of the channel belt. This result has implications for storage times and chemical alteration of floodplain sediments, and the interpretation of measured sediment ages. Our model predictions compare well to data of sediment-age distributions from various field sites and the temporal evolution channel belts observed in flume experiments. The theoretical description of the temporal evolution of channel-belt width developed herein provides a framework in which observational data can be interpreted, and may serve to connect models designed for long and short timescales.



1 Introduction

Rivers migrate laterally. Lateral river migration establishes the channel belt, which is defined as the corridor of channel migration formed during one river-avulsion cycle (Bridge and Leeder, 1979; Nyberg et al., 2023). Channel belts include the river channel and active bars, levees and abandoned channels, and other areas affected by the river during floods or migration (Fig. 1A) (Nyberg et al., 2023). They can be represented by the planform area that the river has interacted with since its last avulsion. During lateral migration, rivers deposit sediment or erode previously deposited sediment, thereby affecting chemical weathering, nutrient transport, and ecology (e.g., Fotherby, 2009; Jonell et al., 2018; May et al., 2013; Miller, 1995; Naiman et al., 2010; Schumm & Lichty, 1963; Torres et al., 2017). Channel belts affect catchment hydrology, host aquifers and hydrocarbon deposits (e.g., Andersen et al., 1999; Blum et al., 2013; Bridge, 2001), and present a key location for organic carbon storage and alteration (e.g., Repasch et al., 2021). Landforms such as backswamps or oxbow lakes, which are specific to channel belts, often host unique ecological communities that depend on regular floods (e.g., Bayley, 1991; Junk et al., 1989; Meitzen et al., 2018). Further, the exchange of sediment during lateral channel migration determines the distribution of ages of the sediment stored at and near the surface along rivers (e.g., Bradley & Tucker, 2013; Pizzuto et al., 2017). Finally, lateral bank erosion is an important natural hazard that can destroy agricultural areas and infrastructure (e.g., Badoux et al., 2014). All of the mentioned effects make channel belts an important component of river response to environmental change (e.g., Hajek and Straub, 2017). As such, they record a river's past activity, and can be used as archives for Earth's history on the timescale of hundreds to thousands of years (e.g., Allen, 1978; Bridge and Leeder, 1979). Channel belts can be either unconfined, for example in foreland areas, or confined, for example by valley walls in mountain regions (Fig. 1 a&b) (e.g., Howard, 1996; Limaye, 2020; Turowski et al., 2024).

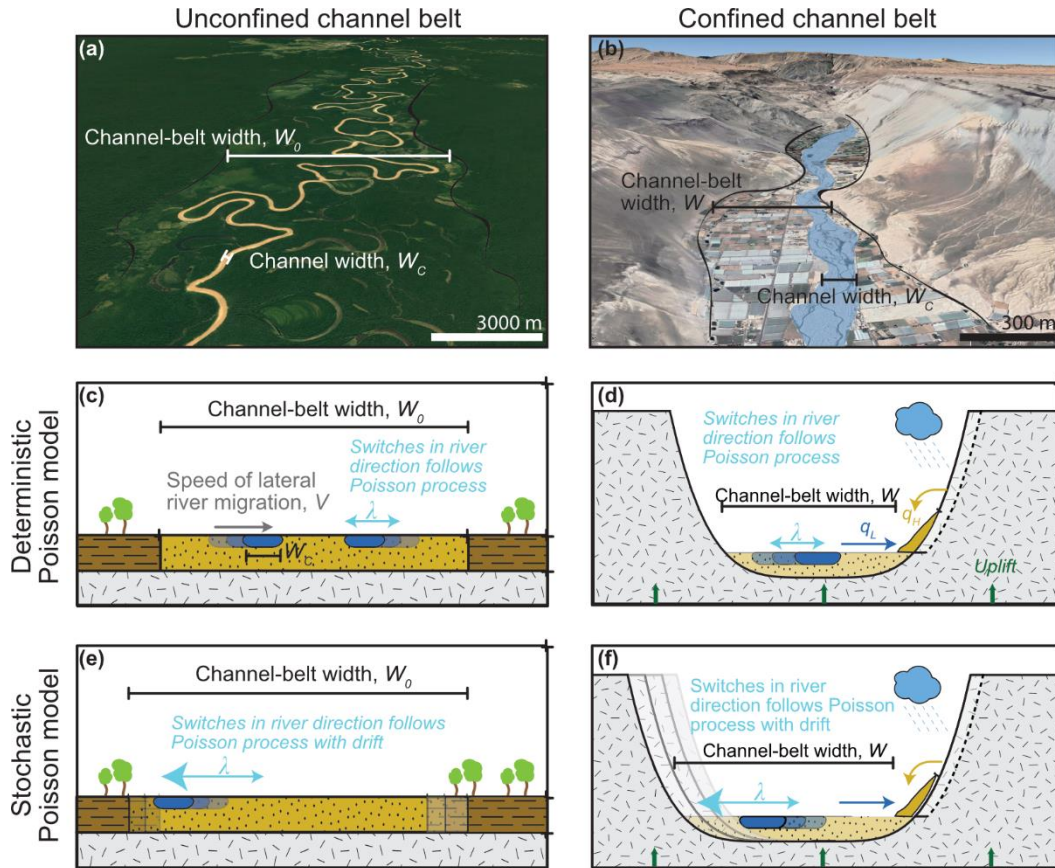
The long-term dynamics of channel belts have been studied separately for meandering (e.g., Camporeale et al., 2005; Greenberg & Ganti, 2024; van de Lageweg et al., 2013) and braided rivers (e.g., Bertoldi et al., 2009; Limaye, 2020). Researchers have largely focused on channel characteristics and statistics, their temporal evolution and approach to a steady state. For meandering rivers, these have typically included the linear and curvilinear wavelength, the curvature of the channel, and the role of meander cuts-offs in reaching and maintaining a steady state (e.g., Camporeale et al., 2005; Howard, 1996). For braiding rivers, they have typically included braiding indices and planform patterns (e.g., Bertoldi et al., 2009; Egozi and Ashmore, 2009). In comparison to these statistics describing the channels within the channel belt, the belt width has received little attention. Greenberg et al. (2024) found that channel-belt area scales with floodplain reworking timescales. Reworking timescales monotonically increase as water partitions into fewer active channel threads, and as channels become more sinuous, and thus vary between river systems with different planform types. Studying models of meandering rivers, Camporeale et al. (2005) concluded that one time and one length scale are sufficient to explain steady state characteristics of channel belts regardless of the hydrodynamic complexity of the underlying model. They suggested that channel-belt width scales with the meandering wavelength, which in turn scales with flow depth. A qualitative comparison to natural channels was favourable.



65 Limaye (2020) postulated that channel-belt width of braided rivers scales with channel width. Using flume experiments, they
showed that both channel and belt width follow a similar scaling relationship with discharge. Turowski et al. (2024) developed
a steady state model for channel-belt and valley width under the assumption that switches in the direction of lateral channel
migration are based on a random process with a uniform mean rate of switching in time. In their model, the unconfined steady
state channel-belt width linearly depends on flow depth. They also suggested that the width of fluvial valleys is controlled by
70 the channel-belt width.

The transient evolution of channel-belt width has so far hardly been explored. Limaye (2020) identified three phases of
channel-belt growth in his experiments, co-occurring with distinct phases of meandering or braiding. In a first phase, the
channel established a graded geometry from the initial imposed boundary condition. In the second phase, the channel belt grew
75 rapidly, while in the third phase, it reduced its growth rate. When compared in a dimensionless framework, the switches
between phases occurred at the same dimensionless time for different experimental conditions. Wickert et al. (2013) and Bufe
et al. (2019) observed an exponential approach to the steady state width in experiments, when tracking the increase of the area
visited by the channel over time. Hancock & Anderson (2000) suggested that the initial rapid widening rate of a channel belt
and the subsequent decrease of the widening rate is due to the declining probability of the channel to be located at the belt
80 boundary as the belt widens. This notion was regularly picked up in subsequent work (e.g., Malatesta et al., 2017; Martin et
al., 2011), and has led to steady state descriptions of valley width (Tofelde et al., 2022; Turowski et al., 2024). Yet, equations
relating the growth evolution of channel belts and valleys to the hydraulic conditions in the channel are currently not available.

Turowski et al. (2024) described lateral channel migration as a Poisson process, in which the switches in direction occur
85 randomly in time at a constant mean rate. They subsequently focused on the mean behaviour of the model, and proceeded to
derive equations for the steady state width of unconfined and confined channel belts, and of fluvial valleys. Here, we explore
the predictions of their model concept for the transient approach of channel belts to their steady state width, and the
consequences of a stochastic formulation for channel-belt dynamics. Specifically, we derive analytical equations describing
the temporal evolution and the bounds of channel belts, their average lateral drift once they have reached a steady state, and
90 the sediment residence-time distribution, which is equivalent to the distribution of sediment ages. Analytical results are
benchmarked with stochastic numerical simulations. We compare the model results to data from flume experiments (Bufe et
al., 2016, 2019), and sediment age distributions from three field sites (Everitt, 1968; Huffman et al., 2022; Skalak & Pizzuto,
2010).



95 **Fig. 1:** Schematic illustration of the model concept. a) Unconfined channel belt of the Juruá River, Brazil (6.75° S, 70.30° W; Map
 data: Google,©2024 Maxar Technologies). b) Confined channel belt of the San Jose River, Chile (18.58° S, 69.97° W; Map data:
 Google,©2024 Maxar Technologies, Airbus). (c, d) the channel switches the direction of motion after a certain timescale. It thus
 evolves to a steady-state width that does not change over time. In the stochastic Poisson model (e, f), the switching timescale is a
 100 random number. As such, the channel may migrate beyond the channel-belt limits (e) or erode the valley walls even after reaching
 the steady-state width. This migration can lead to a lateral drift of the channel belt or valley.

2 Theoretical developments

In this chapter, we will briefly summarize the valley width model by Turowski et al. (2024) (Section 2.1). Afterwards, we
 outline the basis of the stochastic model approach used herein (Section 2.2). Then, we derive equations for the temporal
 evolution of channel belts while approaching a steady state, and their lateral drift speed once they have reached steady state
 105 (Section 2.3), the limits of the channel-belt bounds (Section 2.4), the first passage distribution (Section 2.5), and the age
 distribution of sediment (Section 2.6).



2.1 Summary of the steady state model

Building on earlier work (e.g., Bufo et al., 2019; Martin et al., 2011; Tofelde et al., 2022), Turowski et al. (2024) developed a model for the steady state width of fluvial valleys (Fig 1), which includes predictions for confined and unconfined channel belts as a special case. In the model, each cross-section is treated as if it moves independently from those upstream and downstream. River channels are assumed to move laterally by bank erosion and deposition. The channel belt widens when the river crosses beyond the previous channel belt boundaries (Fig. 1). The lateral channel-migration speed V [$L T^{-1}$] is equal to the ratio of the lateral transport capacity q_L [$L^2 T^{-1}$] and the bank height in the direction of motion H_+ [L], where q_L quantifies the amount of material that the river can move in lateral direction per unit time and channel length (Bufo et al., 2019):

$$V = \frac{q_L}{H_+}. \quad (1)$$

Turowski et al. (2024) viewed switches in the direction of lateral motion of the river as stochastic events. These are independent and identically distributed, with a constant mean event rate per unit time, λ [T^{-1}], and can therefore be described by a Poisson process. The mean rate of switching λ is equal to the ratio of the lateral transport capacity q_L and the square of the flow depth h [L] (Turowski et al., 2024)

$$\lambda = k \frac{q_L}{h^2}, \quad (2)$$

where k [-] is a dimensionless constant. We can define an effective switching time scale. This is a constant time scale that leads to the same steady state width as is obtained from a fully stochastic model. The effective switching time scale ΔT [T] is inversely proportional to λ

$$\Delta T = \frac{c}{\lambda}, \quad (3)$$

where c [-] is a dimensionless constant of order one. Integrating over the distance travelled laterally by the channel within ΔT yields an equation for the unconfined channel-belt width W_0 [L] (see Turowski et al., 2024, for details)

$$W_0 = \int_0^{\Delta T} V dt + W_C = k_0 h + W_C. \quad (4)$$

Here, $k_0 = c/k$ [-] is a dimensionless constant, W_C [L] is the channel width, and t [T] is time. To arrive at the final equality in eq. (4), we assumed that in an unconfined channel belt that is neither incising nor aggrading, the bank height in the direction of motion, H_+ , is equal to the flow depth, h (cf. Turowski et al., 2024). In river valleys, the channel belt or valley floor is narrower than W_0 due to uplift or lateral supply of sediment from hillslopes, and the steady-state valley-floor width W_V [L] can be described by the equation (Turowski et al., 2024):



$$W_V = \left(\frac{q_L - q_H}{U} \right) \ln \left\{ 1 + \frac{U(W_0 - W_C)}{q_L} \right\} + W_C. \quad (5)$$

Here, q_H [L^2T^{-1}] is the lateral supply rate of hillslope sediment per unit channel length, and U [$L T^{-1}$] is the uplift rate. Equation (5) predicts that river valleys reach a steady state width that depends on five input parameters (flow depth h , channel width W_C , uplift rate U , lateral transport capacity q_L , and lateral hillslope sediment supply q_H) and one constant (k_0) that needs to be determined from observations. Steady state valley width is reached when the system achieves a balance between local sediment input from hillslopes and by uplift, on one hand, and the removal of sediment by the river, on the other hand.

In summary, in their model, Turowski et al. (2024) assume that the switches in river direction follow a Poisson process and unconfined channel belts evolve to a steady-state width determined by flow depth and channel width (eq. 4). Fluvial valleys can attain a maximum steady state width that corresponds to the unconfined channel-belt width W_0 . They are narrower than this unconfined width if they are affected by uplift or lateral hillslope sediment supply (eq. 5). We call this model the ‘Deterministic Poisson model’ hereafter.

2.2 The Stochastic Poisson model

In order to investigate the transient evolution of channel-belt width, we further develop the previous model of Turowski et al. (2024). Instead of summarizing the channel switches with a constant characteristic timescale, the effective switching timescale ΔT (eq. 3), we now explore the consequences of a random switching timescale. This consideration allows us to observe the transient behaviour of the random-walk model for lateral river migration. We call this model the ‘Stochastic Poisson model’ hereafter. In a Poisson process, the probability mass function (PMF) that n [-] events (in this case, channel switches) occur within the average switching timescale Δt [T] is given by

$$\text{PMF}_{\text{Poisson}} = \frac{(\lambda \Delta t)^n e^{-\lambda \Delta t}}{n!}. \quad (6)$$

The expected number of events is given by $1/(\lambda \Delta t)$ [-] and the variance by $\lambda \Delta t$ [-]. For the derivations within this paper, we use the idea that the lateral motion of the river channel across the floodplain, in the model concept of a Poisson process, can be viewed as a non-standard one-dimensional random walk. The channel alternates between steps to the left and to the right within the cross section, thus switching direction after every step. The step length is not a constant, but a stochastic parameter equal to the waiting times between individual switching events multiplied by lateral migration speed. In a Poisson process, the waiting times T_W [T] between events are exponentially distributed with a mean waiting time of $1/\lambda$, a variance of $1/\lambda^2$, and a probability density function (PDF) given by

$$\text{PDF}_{\text{exponential}} = \lambda e^{-\lambda T_W}. \quad (7)$$

Similarly, for constant migration speed V [$L T^{-1}$], the PDF of the length of steps $\Delta x = V \Delta t$ [L] is given by



$$\text{PDF}_{\text{exponential}} = \frac{\lambda}{V} e^{-\frac{\lambda}{V} \Delta x}. \quad (8)$$

170 In the following, we will first derive an equation for the approach to the steady state width using the ‘Deterministic Poisson model’ (Turowski et al., 2024), and then use the mathematics of random walks to explore the effects of stochasticity on the channel belt’s temporal evolution. Finally, we investigate the distribution of floodplain ages.

2.3 Temporal evolution of the channel-belt width

2.3.1 Approach to steady state in the ‘Deterministic Poisson model’

175 We first consider the evolution of the channel belt in an unconfined setting. Consider the river channel moving laterally with speed V . The channel belt widens when the river is located at and moves into the channel-belt boundary. In contrast, if the river is not located at the boundary, or moves away from it, the channel-belt width remains unchanged. At any given time, widening can be observed with a probability P [-], which is equal to the fraction of the time the river spends widening the valley (e.g., Hancock and Anderson, 2002; Tofelde et al., 2022). The temporal evolution of channel-belt width W [L] is then
180 governed by the differential equation (Tofelde et al., 2022)

$$\frac{dW}{dt} = PV. \quad (9)$$

Motion in either direction is equally likely, and, for a given set of hydraulic, tectonic, and sedimentological boundary conditions, V can be considered as a constant (Bufe et al., 2019; Turowski et al., 2024). In a transient phase, before the steady
185 state width is reached, the probability of the river not widening (i.e. $1-P$) the channel belt is equal to the ratio of the current W [L] and the maximum W_0 [L] channel-belt width (Tofelde et al., 2022). Channel width W_C provides a starting point and needs to be subtracted. Thus, P is given by (Turowski et al., 2024)

$$P = 1 - \frac{W - W_C}{W_0 - W_C} = \frac{W_0 - W}{W_0 - W_C}. \quad (10)$$

190 The speed of lateral motion is equal to the ratio of the lateral transport capacity and the height of the bank in the direction of motion H_+ (eq. 1). Combining eqs. (1), (9) and (10), we obtain a differential equation for channel-belt evolution

$$\frac{dW}{dt} = \frac{W_0 - W}{W_0 - W_C} \frac{q_L}{H_+}. \quad (11)$$

Solving equation (11) and applying the boundary condition that channel-belt width W is equal to W_C at time $t = 0$, we obtain

195

$$W(t) = W_0 - (W_0 - W_C) \exp\left\{-\frac{t}{\tau}\right\} + W_C. \quad (12)$$



Here, τ is the governing timescale, which can be interpreted as a response time scale to an external perturbation (c.f. Tofelde et al., 2021). It is given by

$$\tau = (W_0 - W_C) \frac{H_+}{q_L}. \quad (13)$$

200

Assuming that H_+ is equal to flow depth h and substituting eqs. (1) and (2) into eq. (11), we find that τ is equal to the effective switching time scale ΔT (see eqs. 3 and 4):

$$\tau = \frac{c}{\lambda} = \Delta T. \quad (14)$$

205

We can use a similar approach to describe the evolution of a channel belt that is confined by valley walls when considering that at the valley walls, the lateral migration of the river slows down (cf. eq. 1). If the valley walls are made of alluvium, the bank height H_+ in eq. (9) is equal to the height of the valley wall H_W [L] and eq. (1) can be used as before. However, we need to adjust eq. (10), defining an equivalent probability $P_{confined}$ for a confined channel belt. The distance d [L] is the length that a channel moves on average across the valley floor in the effective time ΔT [T] between two events of switching the direction of motion. This distance d is the sum of the distance covered at higher speed V when moving in the floodplain, and the distance covered when moving at lower speed v [L/T] when cutting into the valley walls (cf. Tofelde et al., 2022)

210

$$d = V(1 - P_{confined})\Delta T + vP_{confined}\Delta T. \quad (15)$$

For the unconfined channel belt, we know that

215

$$V\Delta T = W_0 - W_C. \quad (16)$$

Using eq. (16) to eliminate ΔT in eq. (15), and noting that d corresponds to the current width $W - W_C$, we obtain

$$P_{confined} = \frac{W_0 - W}{(W_0 - W_C) \left(1 - \frac{v}{V}\right)} = \frac{W_0 - W}{(W_0 - W_C) \left(1 - \frac{H_W}{h}\right)}. \quad (17)$$

220

Here, we used eq. (1) to substitute for V and v , using $H_+ = h$ and $H_+ = H_W$, respectively. Note that in the assumption behind eqs. (15) to (17), $P_{confined}$ for a confined valley (eq. 17) reduces to P for an unconfined floodplain (eq. 8) for $v = 0$ or $H_W = 0$ (rather than $v = V$ or $H_W = h$). This arises from eq. (15), which yields $d = V\Delta T$ for $v = V$, rendering $P_{confined}$ meaningless. Substituting eq. (17) into eq. (9) and integrating again yields eq. (12) with a different governing timescale τ given by

$$\tau = \frac{(W_0 - W_C)(H_W - h)}{q_L} = \left(\frac{H_W}{h} - 1\right) \frac{c}{\lambda} \quad (18)$$

225



2.3.2 Channel belt evolution in the ‘Stochastic Poisson model’

As we did in Section 2.3.1, we first consider the evolution of the channel belt in an unconfined plane. In the ‘Deterministic Poisson model’, we obtained an exponential approach to the steady state width (eq. 12) (Section 2.3.1). In the ‘Stochastic Poisson model’, we can distinguish three different phases in the growth of the channel-belt width over time. In the first phase, before the first switch in direction occurs, width increases linearly in time. In this phase, the growth rate is determined by the speed of lateral channel migration, V in the unconfined case and v in the confined case (see eq. 1 and Section 2.3.1). In the second phase, before reaching the steady state width, the channel-belt width grows exponentially on average. This average exponential growth can be described by the same equation (eq. 12) that has been derived for the ‘Deterministic Poisson model’ (see Section 2.3.1). In the third phase, which starts approximately when the width for the first time reaches the steady state width, stochastic drift dominates. Stochastic drift arises, because, due to the random motion of the channel, there is always a finite probability to widen the belt even after the steady state width has been reached. We already have equations for the linear (eq. 1) and the exponential (eq. 12) phase. In the following, we will fully exploit the stochastic properties of the model concept. In several of our considerations in this and the following sections, we use the central limit theorem, which states that the sum X of n stochastic variables with mean μ and variance σ^2 is normally distributed with mean $n\mu$ and variance $n\sigma^2$ if n is sufficiently large. In addition, we use the result that the sum or difference of two normally distributed parameters with means μ_1 and μ_2 and equal variance σ^2 follow a normal distribution with mean $\mu_1 \pm \mu_2$ and variance $2\sigma^2$.

First, we will derive an equation for widening during the drift phase using the evolution of random walks in the limit of a large number of steps. In this case, we can apply the central limit theorem. Thus, the PDF of the location of the channel can then be described by a normal distribution. In a random walk, the width of this normal distribution increases with the square root of its variance $\text{VAR}_{UCB} [L^2]$, where the subscript stands for ‘unconfined channel belt’ (e.g., Lawler & Limic, 2010):

$$W_{Drift} = \sqrt{\text{VAR}_{UCB}} + W_C. \quad (19)$$

To find an equation for the variance, we will use the concept of a random walk making steps in alternating directions with exponentially distributed step length. We consider m pairs of a total of n steps, where each of the n steps covers an average distance of V/λ . The difference of two consecutive identically exponentially distributed steps in opposite directions is described by the Laplace distribution with zero mean and variance $2V^2/\lambda^2$, with the PDF

$$\text{PDF}_L = \frac{\lambda}{2V} e^{-\frac{\lambda}{V}|x|}. \quad (20)$$

After each pair of two steps, the river is always in a position where it switches direction in the same way, for example from left to right. The switch in the other direction, from negative to positive, also follows eq. (20). In the limit of large m , the position of the river is given by the sum of the positions of many step pairs. The central limit theorem applies, and the normal approximation gives the distribution of locations where the river switches either from positive to negative or vice versa, with zero mean and a variance of $2mV^2/\lambda^2 = nV^2/\lambda^2$. Finally, the channel-belt width is the difference of the switching position



on either side, so the final variance needs to be multiplied by a factor of two. Applying the law of large numbers, the distance
260 covered in the sum of all steps is equal to the number of steps times the average step length V/λ . The average time of each step
is the mean waiting time $1/\lambda$, and so we can write $n = \lambda t$:

$$\text{VAR}_{UCB} = 2n \frac{V^2}{\lambda^2} = 2 \frac{t}{\lambda} V^2 = \frac{2}{k} q_L t. \quad (21)$$

Thus, we obtain the drifted distance or the width increase due to drift from eqs. (19) and (21) as

$$W_{Drift}(t) = \sqrt{\frac{2}{k} q_L t} + W_C. \quad (22)$$

For a confined channel belt, during the time the river incises into the confining walls, the speed of widening drops to q_L/H_W ,
where H_W is the height of the confining wall, while it remains at q_L/h , as before, when the river moves laterally within the
channel belt. The average speed of motion is given by the geometric average of the two speeds, \bar{V}

$$\bar{V} = \sqrt{vV} = \sqrt{\frac{h}{H_W}} V. \quad (23)$$

We obtain the variance by replacing V by \bar{V} in equation (22), giving the variance VAR_{CCB} for a confined channel belt

$$\text{VAR}_{CCB} = 2t \bar{V}^2 / \lambda = 2q_L t h / k H_W \quad (24)$$

275 As before, the width during the drift phase evolves as the square root of the variance, giving

$$W_{Drift}(t) = \sqrt{2 \frac{t}{\lambda} \bar{V}^2} + W_C = \sqrt{\frac{2}{k} \frac{h}{H_W} q_L t} + W_C. \quad (25)$$

2.3.3 Drift speed of channel belts and dimensionless scaling factor of the mean switching time scale

During the drift phase, the channel belt widens laterally, increasing the area that has been reworked by the channel with the
280 square root of time (eq. 25). Yet, growth on one side of the channel belt makes it less likely that the channel moves close to
the other side. As such, parts of the channel belt may be abandoned and, for example, reclaimed by vegetation (Fig. 1E).
Similarly, in the case of a vertically incising river, the channel-belt width can stay at the steady state value W_V (eq. 5), while
the entire belt is moving laterally, and uplift converts old parts of the channel belt to fluvial terraces. Here, we consider the
case that the channel belt keeps its width constant at the steady state width, because any acquisition of area of the belt due to
285 lateral motion on one side leads to the abandonment of an equivalent area on the other side. In this case, instead of widening,
during the drift phase, the entire belt drifts laterally. We will now derive an equation for the average drift speed in this case.



The average drifted distance in one direction, X_{Drift} , is equal to the square root of the variance, as before (cf. eq. 19). Because we consider a distance, rather than the width, it is smaller by a factor of two in comparison to eq. (25), giving

$$X_{Drift}(t) = \sqrt{\frac{1}{k} \frac{h}{H_W} q_L t}. \quad (26)$$

290

The derivative of eq. (26) with respect to time, evaluated at the time when the valley reaches its steady state width, T_{SS} [T], gives the drift speed V_{Drift} [LT^{-1}]

$$V_{Drift} = \frac{1}{2} \sqrt{\frac{1}{k} \frac{h}{H_W} \frac{q_L}{T_{SS}}}. \quad (27)$$

295 At time T_{SS} , X_{Drift} is equal to the steady state width W_0 , and we can use eq. (26) to obtain

$$T_{SS} = k \frac{H_W (W - W_C)^2}{h 2q_L}. \quad (28)$$

Substituting eq. (28) into eq. (27) yields

$$V_{Drift} = \frac{1}{\sqrt{2k}} \frac{h}{H_W} \frac{q_L}{(W - W_C)}. \quad (29)$$

300

We can use eq. (29) to calculate the constant of proportionality c between the switching time scale ΔT and the rate constant λ (eq. 3). The ratio of the drift speed V_{Drift} and the lateral migration speed of the channel V is the same as the fraction of time that the river spends widening the channel belt. This is equal to the area under a normal distribution outside one standard deviation from the mean, $V_{Drift}/V = 0.3173$. Setting $h/H_W = 1$ and substituting $q_L = Vh$, we find

$$\frac{V_{Drift}}{V} = 0.3173 = \frac{1}{\sqrt{2k}} \frac{h}{(W - W_C)} = \frac{1}{\sqrt{2c}}. \quad (30)$$

305

Equation (30) therefore yields $c = 2.2285$.

2.4 Channel-belt limits

310 We can use the properties of random walks to make a statement about the distance beyond which the river will rarely migrate over a given timescale. Knowledge of this distance may be useful to delineate zones for building, or to assess in which areas the river is likely (or not) to interact with its surrounding, for example, by reworking sediment or evacuating erosion and weathering products. In random walks, this distance is described by the law of the iterated logarithm (e.g., Kolmogoroff, 1929), which is a limit theorem that sits somewhere in between the central limit theorem and the law of large numbers. In the limit of
315 a large number of steps, this law provides an envelope to the area that the river almost surely will not leave in its stochastic



motion. Consider the sum S over the distance travelled in n steps over dimensionless time t^* , which is a dimensionless stochastic variable with zero mean. The law of the iterated logarithm gives an upper and lower bound for this sum with the equation

$$S = \pm \sqrt{2t^* \ln\{\ln\{t^*\}\}}. \quad (31)$$

320 Here, \ln denotes the natural logarithm, and the plus and minus give the upper and lower bound, respectively. We define the dimensionless step length $s = \lambda \Delta x / V$. This step length is a stochastic variable that is exponentially distributed with a mean of zero and variance equal to one (compare to eq. 7). Because the random walk has to be symmetric for eq. (31) to apply, we consider the sum S of $m = n/2$ pairs of steps, distributed according to the Laplace distribution (eq. 15). Normalizing with the square root of the variance of the Laplace distribution, the dimensional distance is then given by $X = \sqrt{2}SV/\lambda$. This is the distance from the origin that the channel will almost surely not cross within timescale t . The dimensionless time is given as $t^* = 2Vt/h$, where the factor of two accounts for the pairs of steps. Putting everything together and adding half of the channel width, we obtain

$$X(t) = \sqrt{2} \frac{SV}{\lambda} + \frac{W_c}{2} = \pm 2 \frac{h}{k} \sqrt{2 \frac{\lambda t}{k} \ln\left\{\ln\left\{2 \frac{\lambda t}{k}\right\}\right\}} + \frac{W_c}{2}. \quad (32)$$

330 2.5 First passage time distribution

We can derive another result that may be useful for planning and hazard mitigation purposes over long time scales, when considering regular, effective floods. The first passage time distribution (e.g., Redner, 2001) is the distribution of times until the channel reaches a point that is located a distance b [L] from the channel's original location for the first time. This time distribution can be used, for example, to calculate lifetime distribution of structures a distance b from the river. In random walks, the first passage time distribution is given by a Lévy distribution. The distribution PDF_{FP,R} of times T_{FP} [T] is given by:

$$\text{PDF}_{FP,R}(T_{FP}) = \frac{|b|}{\sqrt{2\pi \frac{h}{H_W} \frac{q_L}{k} T_{FP}^3}} \exp\left\{\frac{-b^2}{2 \frac{h}{H_W} \frac{q_L}{k} T_{FP}}\right\}. \quad (33)$$

2.6 Sediment residence-time distribution

The probability distribution of residence times may be useful to calculate the age distribution of sediments. This is relevant, for example, for understanding weathering rates in river deposits or transfer times of carbon to the ocean (e.g., Repasch et al., 2021; Tofelde et al., 2021). The residence time distribution differs from the first passage distribution (Section 2.5), but can be derived from it. We start with a single step outward. The migrated distance Δx until the channel switches direction is then



345 given by the exponential distribution (eq. 8). We can then use the first passage distribution (eq. 33) for the time to return to the origin by migrating again a distance $b = \Delta x$. Finally, we need to account for all possible Δx in the initial step. Assuming that the first step has to erode into the valley walls, the distribution PDF_{RT} for the time needed to return to the origin T_R [T] is then given by

$$\text{PDF}_{RT}(T_R) = \int_0^{\frac{h}{HW}Vt} \frac{\lambda}{\frac{h}{HW}V} \exp\left\{\frac{-\lambda}{V} \Delta x\right\} \frac{|\Delta x|}{\sqrt{2\pi \frac{h}{HW} \frac{qL}{k} \left(T_R - \frac{\Delta x}{\frac{h}{HW}V}\right)^3}} \exp\left\{\frac{-\Delta x^2}{2 \frac{h}{HW} \frac{qL}{k} \left(T_R - \frac{\Delta x}{\frac{h}{HW}V}\right)}\right\} d\Delta x. \quad (34)$$

Unfortunately, eq. (34) does not yield an analytical solution. However, we can find an analytical limit for the right-hand tail, when T_R is large. Then, the integral reduces to

$$\text{PDF}_{RT}(T_R \gg 0) = \int_0^\infty \frac{\lambda}{\frac{h}{HW}V} \frac{|\Delta x|}{\sqrt{2\pi \frac{h}{HW} \frac{qL}{k} (T_R)^3}} \exp\left\{\frac{-\lambda}{V} \Delta x\right\} d\Delta x = \frac{\lambda}{\sqrt{2\pi}} \left(\frac{h}{HW} \lambda T_R\right)^{-3/2}. \quad (35)$$

We suggest an analytical approximation for the entire distribution (eq. 34) by assuming that, for small T_R , the PDF approaches a constant. Using this condition together with eq. (35) and fixing the integral to one, as required for any distribution, we obtain the function

$$\text{PDF}_{RT}(T_R) \approx \frac{1}{\sqrt{2\pi}} \frac{a\lambda}{1 + a(\lambda T_R)^{3/2}} \quad (36a)$$

with

$$a = \left(\frac{3}{2}\right)^3 \left(\frac{3}{2\pi}\right)^{3/2}. \quad (36b)$$

3. Comparison to numerical model, experiments and field data

We use a stochastic random walk model to benchmark and check the analytical equations (Section 3.1). Results are compared to two separate types of data: (i) published distributions of floodplain sediment ages (Section 3.2) (Everitt, 1968; Huffman, 2022; Skalak & Pizzuto, 2010), and (ii) the temporal evolution of channel belts in the experiments of Bufe et al. (2016a,b, 2019) (Section 3.3).



3.1 Numerical model

We used a stochastic numerical random walk model, specifically a non-standard random walk with non-uniform, exponentially distributed step length in alternating directions. Except where otherwise stated, we fixed channel width to zero, and all other free model parameters to one. For each time step, the step length was randomly picked from an exponential distribution (eq. 7), and the lateral position of the channel was tracked by alternately adding or subtracting the obtained step length from the channel's previous position. Channel-belt width was calculated as the difference of the maximum distance that the channel had migrated into in the positive and negative directions from the origin up to the time step of interest. In this way, we generated a total of 1,000 trajectories of position and channel-belt width, each with a total length of 3,000 time steps. We repeated this exercise for ratios of valley depth to channel depth of $H_w/h = 1, 10$ and 100 . We obtained the average position of the channel for bins spaced logarithmically in time. We used the unconfined width in further simulations to check the drift equation (eq. 25). For this check, we ran the random walk, limiting the channel-belt width to the steady-state width by adjusting the other side of the valley in an equal manner when one side of it was eroded. This procedure results in a valley of fixed width that moves laterally. We measured drift velocity for different steady state widths by varying the channel depth, for different values of the lateral transport capacity, and, as above, for ratios of valley depth to channel depth of $H_w/h = 1, 10$ and 100 . These simulations were run for a total of 3,000 time steps to ensure statistical convergence. To verify the dimensionless scaling factor c that relates the mean switching time to the rate constant λ by c/λ , we compared the unconfined steady state width for various conditions to flow depth (eq. 2) for simulations with $k = 1$. To obtain an independent estimate of W_0 from the data, we fitted the exponential evolution equation (eq. 12) to the initial phase of channel-belt widening. To obtain the distribution of channel belt ages, we ran the same random walk simulations until the channel returned to the origin for the first time. We repeated the simulation 10,000 times, for a maximum of 100,000 steps. The times needed to return to the origin in each run was used to construct the distribution of sediment residence times. Similarly, to test the first passage distribution, we ran 10,000 simulations, each until the walk reached a distance of 10 from the starting point. All scripts are available in the publication by McNab (2024).

3.2 Floodplain ages

We digitised floodplain ages published by Everitt (1968), Skalak & Pizzuto (2010), and Huffman et al. (2022) to compare against the predicted power-law scaling (eq. 35). In the original study of Skalak & Pizzuto (2010), the cumulative distribution function (CDF) of floodplain ages is shown (their Figure 8). We estimated the PDF by numerically differentiating the CDF using a centred finite-difference scheme.

3.3 Experiments

Bufe et al. (2016a) and Bufo et al. (2019) conducted and analysed experiments on braided alluvial channels in a basin with dimensions of $4.8 \times 3.0 \times 0.6$ m and filled with well-sorted silica sand ($D_{50} = 0.52$ mm). Water and sediment were supplied into



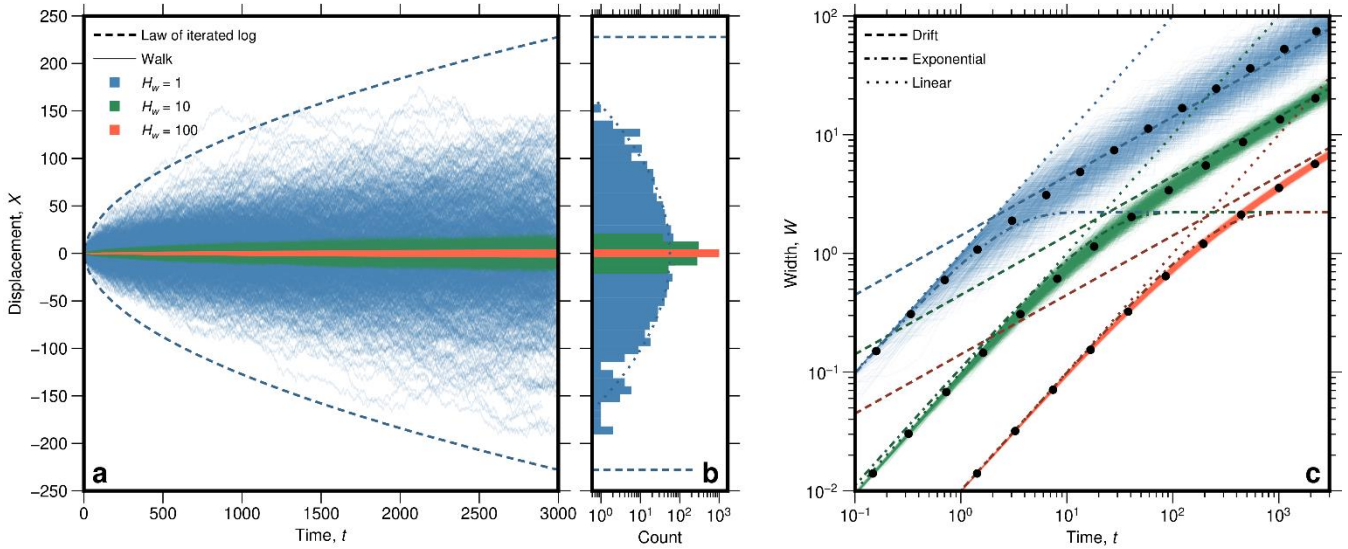
the basin at a constant rate from the centre of one of the short edges, and flowed out of the opposite side of the basin across a weir into a drain. After the start of the experiments, the system evolved into an aggrading braided channel network. Once the average aggradation rate dropped to below 20% of the input flux, a flexing metal sheet underneath the basin was used to simulate an uplifting fold. Here, we focus on 25 hours of data that was collected before the onset of uplift from Run 5, and on 400 55 hours of data from Run 7, an experiment without uplift (see Bufe et al., 2019, for more detail). Water discharge was set to 790 ml/s in both experiments and sediment supply was 15.8 ml/s in Run 7 and 2.4 ml/s in Run 5. Positions of the channels were tracked at one-minute intervals in overhead images by using blue-dyed water (Bufe et al., 2016a) and were used to measure the rate at which the area reworked by the channel expanded over time.

405 4. Results

In general, our analytical solutions (section 2) agree well with the Monte-Carlo simulations of the random walks (section 3.1) (Figs. 2-6). The law of the iterated logarithm (eq. 32) gives an upper bound on the locations of the channel through time (Fig. 2a,b, Fig. 5a, Fig. 6a), and we can identify all three phases – linear, exponential and square root drift – in the temporal evolution of width (Fig. 2c). The lateral drift velocity of valleys at steady state is inversely proportional to valley width and proportional 410 to the lateral transport capacity (Fig. 3), as expected from eq. (29). The theoretical value of the constant $c = 2.2285$ (eq. 30) could be verified by the simulations (Fig. 4). The first passage distribution (eq. 33) provides a good description for the simulation results (Fig. 5). The analytical approximation of the age distribution (eq. 36, Fig. 6) underpredicts the modelled ages for small ages, but provides an exact description of the right-hand power-law tail (Fig. 6b). The age data from Everitt (1968), Skalak & Pizzuto (2010), and Huffman et al. (2022) are consistent with the $-3/2$ power-law scaling (eq. 35) (Fig. 6c).

415

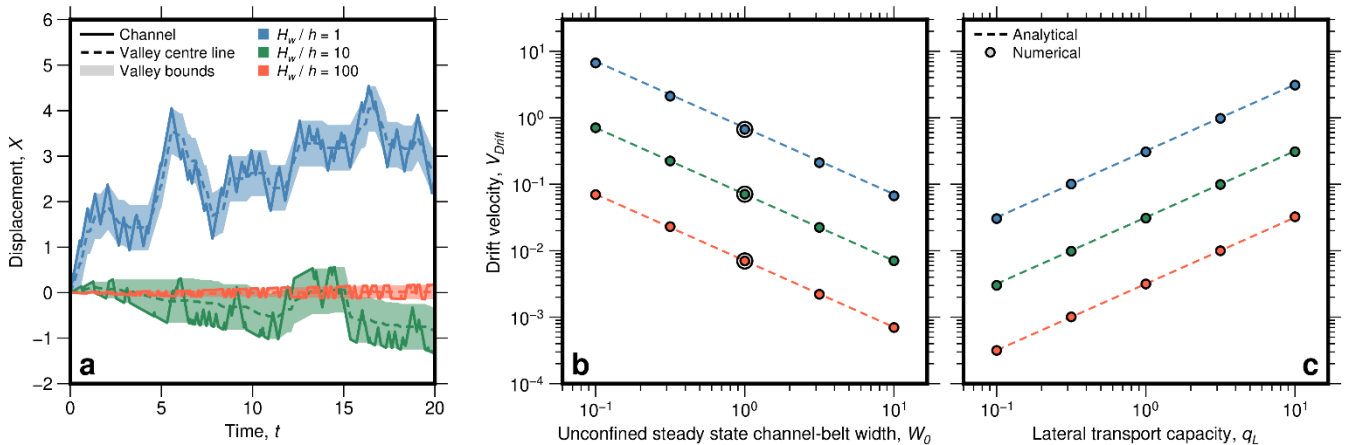
In the evolution of the experimental channel belts, we can clearly identify a drift phase (Fig. 6). This phase is apparent as a square root scaling of channel-belt width as a function of time (eq. 25). We find $q_l/k = 2.15 \times 10^{-5} \text{ m}^2/\text{s}$ for Run 5 and $q_l/k = 2.62 \times 10^{-5} \text{ m}^2/\text{s}$ for Run 7.



420

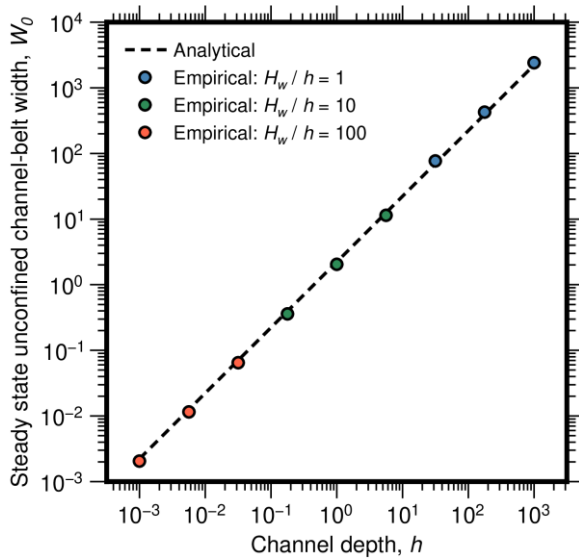
Fig. 2: Temporal evolution of channel-belt width in the numerical experiments. a) Modelled migration paths through time, bounded by the law of the iterated logarithm (eq. 32), with the location density at $t = 3000$ shown in b). The dotted line on b) gives the theoretically expected normal distribution for the unconfined case (blue). c) Average width evolution, showing the analytical expressions for the linear (eq. 1), exponential (eq. 12) and drift phases (eq. 25). Black circles show mean widths in bins spaced logarithmically in time. Standard errors of the means are smaller than the symbols.

425

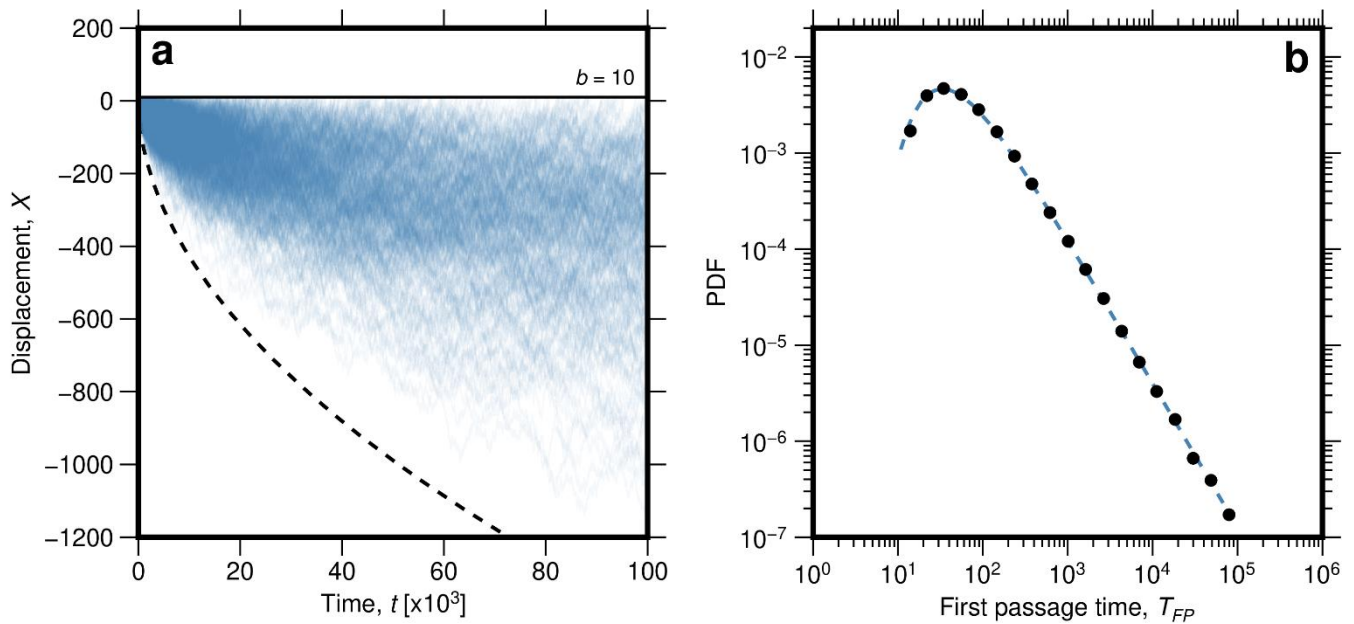


430

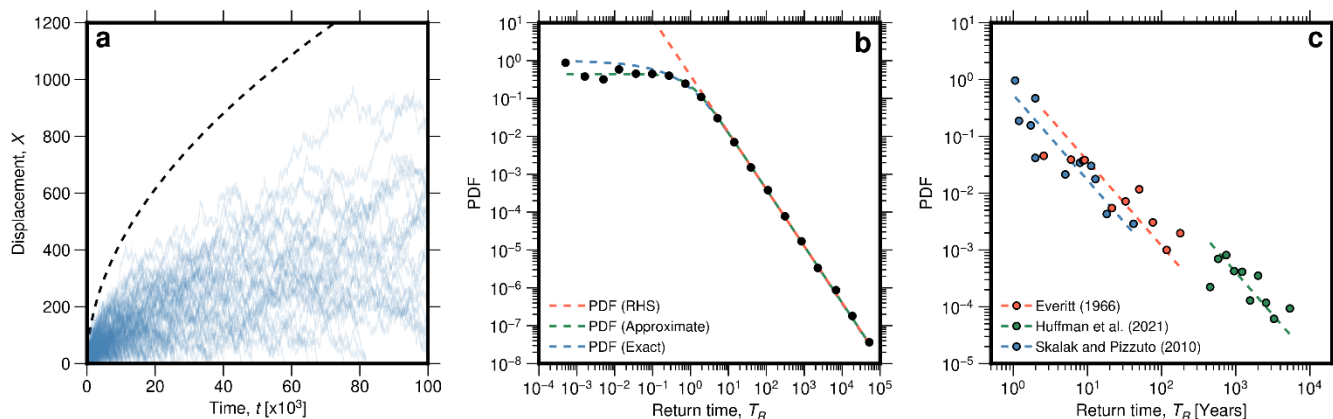
Fig. 3: Lateral drift of channel belts in a steady state. For the calculation, channel-belt width was fixed to the steady state width, i.e., whenever the channel widened the channel belt on one side, the width was reduced by the same amount on the other side. a) Channel location as a function of time for cases of H_w/h . Average drift velocity as a function of b) steady width and c) lateral transport capacity confirm the analytical predictions of eq. (29). Larger circles show simulations plotted in a). Note that a) does not show the entire calculated trajectories. Average drift velocities in b) and c) were measured after 10,000 steps.



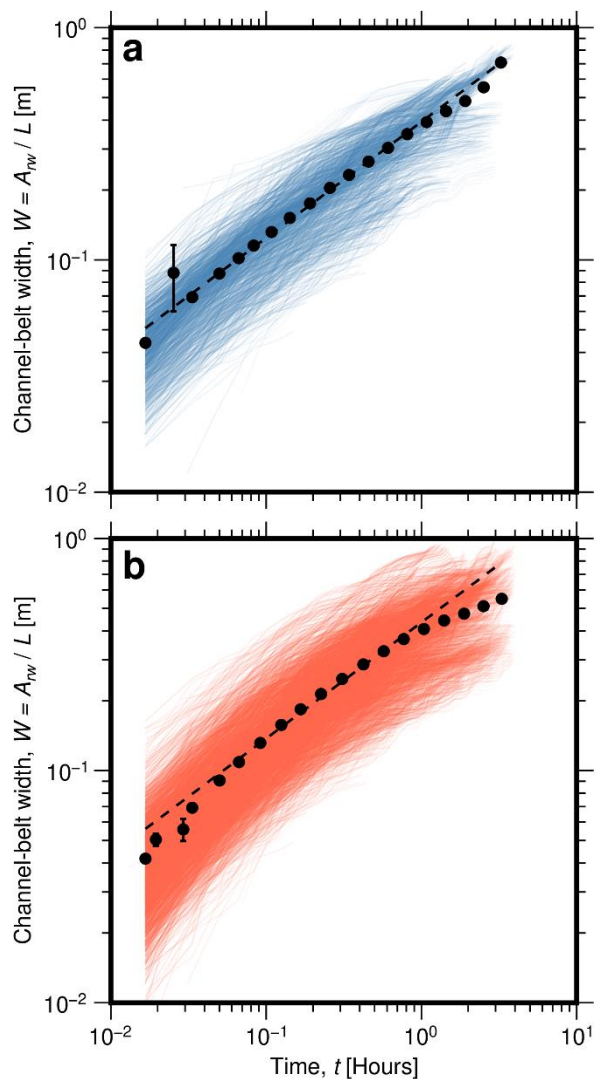
435 **Fig. 4:** Verifying the value of the constant c (see eq. 30) by comparing unconfined steady state channel-belt width to channel depth for varying simulations. We set channel width $W_C = 0$ and $k = 1$ for these simulations. Then, the steady state channel-belt width and flow depth should be proportional with a constant of proportionality equal to $1/c$ (eq. 4). The blue dashed line gives the theoretically expected relationship with $c = 2.2285$ (eq. 30). The results also show that the value of c is the same for unconfined and confined channel belts.



440 **Fig. 5:** The analytical results for the first passage distribution. a) Paths of models to investigate time distribution to reach a point a distance b from the origin. The dashed line gives the law of the iterated logarithm (eq. 32). In comparison to Fig. 2a, substantially longer runs in time are shown here. b) Modelled time distribution in comparison to the exact solution (eq. 33).



445 **Fig. 6: The analytical results for the return time distribution, equivalent to the age distribution of sediments stored in the channel**
belt. a) Paths of models to investigate time distribution for the return to the origin. The dashed line gives the law of the iterated
logarithm (eq. 32). In comparison to Fig. 2a, substantially longer runs in time are shown here. b) Modelled time distribution in
comparison to the exact solution (blue, eq. 34), the power law decay in the right-hand tail with an exponent of $-3/2$ (red, eq. 35). The
analytical approximation (green, eq. 36) is also shown. c) Data from Everitt (1968), Skalak & Pizzuto (2010), and Huffman et al.
 450 **(2022) are consistent with the $-3/2$ power law tail.**



455 **Fig. 7: Temporal evolution of the cumulative inundated area in the experiments, with data from a) Run 5 (blue) and b) Run 7 (red). Black dots give binned means, and error bars show the standard errors of the means (mostly smaller than the symbols). The dashed line is the fitted square root relationship with time that can be expected for the drift phase (eq. 25).**

5. Discussion

5.1 Model predictions and overview

Using the Poisson concept for the formation and evolution of channel belts, we derived a range of results that hold implications for fluvial geomorphology, quantitative landscape evolution studies, and river management (Table 1). The stochastic treatment allowed us to theoretically quantify one of the two unconstrained parameters in the model of Turowski et al. (2024). As such, apart from the factor of proportionality k in the definition of the switching timescale λ (eq. 2), all of the model parameters can



be directly related to channel geometry and hydraulics. In particular, to parameterize the model, one needs measurements of flow depth h , channel width W_C , and the lateral transport capacity q_L . The former two have been routinely measured in the field. Yet, natural river discharge changes over time, and it is currently unclear which flood size is responsible for setting the channel belt in the long-term channel dynamics. The lateral transport capacity depends on discharge, sediment supply and granulometry of a particular river (Bufe et al., 2019). The precise dependence is debated (e.g., Bufo et al., 2019; Constantine et al., 2014; Ielpi and Lapôtre, 2019; Wickert et al., 2013), and likely depends on the characteristics of the particular river, for example its planform type (Greenberg et al., 2024; Nyberg et al., 2023).

The investigated measured age distributions are consistent with the predicted $-3/2$ power law scaling. This will be discussed in detail in section 5.3. The evolution of average channel-belt width in experiments shows the square root scaling with time, as expected for the drift phase (Fig. 7). The exponential approach can be fitted independently (see Bufo et al., 2019). However, the data resolution is not good enough to fit both relationships with consistent parameter values. Essentially, the resulting unconfined channel-belt width W_0 depends on the subjective choice of which data points to include into the fit.

Table 1: Overview of the analytical equations

Result	Comment	Equation #
Channel lateral migration speed	Suggested by Bufo et al. (2019) from experimental data.	1
Average switching rate	Derived by Turowski et al. (2024).	2
Unconfined steady-state channel-belt width	Derived by Turowski et al. (2024).	4
Steady-state valley width	Includes uplift and lateral sediment supply as additional input parameters in comparison to eq. (4). Derived by Turowski et al. (2024).	5
Exponential approach to steady state	The governing time scale for the unconfined case is given by eqs. (13) and (14), and for the confined case by eq. (18).	12
Square root widening	Average increase of area affected by the channel in the drift phase, after the steady state width has been reached.	25
Average drift speed	Average drift speed in the drift phase, assuming the channel belt keeps a constant width.	29
Channel-belt limits	Law of the iterated logarithm as an envelope to the area that the channel is unlikely to leave. Only valid for unconfined channel belts.	32
First-passage time distribution	Distribution of times needed to reach a point a distance b from the origin.	33



Distribution of times needed to return to the origin	This is equivalent to the sediment residence-time distribution, or the age distribution of sediments, assuming a single deposition and remobilisation. The integral equation does not have an analytical solution. An analytical solution for the right-hand tail is given in eq. (35), and an analytical approximation for the entire distribution in eq. (36).	34
--	--	----

5.2 The effect of uplift

In our model derivations, we have not explicitly considered the role of uplift or net incision on the channel-belt width. Uplift increases the bank height encountered by the channel in lateral motion (eq. 1) and thereby slows it down. Turowski et al. (2024) included uplift in their steady state valley-width model and demonstrated that a competition between uplift and lateral mobility of the channel, described by the lateral transport capacity, determines the final width of the valley. Yet, the inclusion of uplift in the stochastic treatment developed herein would introduce considerable complexities into the equations. It seems unlikely that analytical solutions are possible. Here, we suggest a simple approach to circumvent this problem. We equate eqs. (5) and (40) to define an effective lateral migration speed \overline{V}_U [LT⁻¹] in an uplifted area

$$W = \frac{c\overline{V}_U}{\lambda} + W_C = \frac{q_L}{U} \ln \left\{ 1 + \frac{U(W_0 - W_C)}{q_L} \right\} + W_C. \quad (37)$$

Solving for \overline{V}_U , this yields

$$\overline{V}_U = \frac{k V^2}{c U} \ln \left\{ 1 + \frac{U(W_0 - W_C)}{q_L} \right\} \quad (38)$$

We thus obtain an effective variance

$$\begin{aligned} VAR &= \frac{2}{k} \frac{h}{H_W} \frac{\overline{V}_U^2}{\lambda} t = \frac{2}{k} \left(\frac{k}{c}\right)^2 \frac{h}{H_W} \frac{V^4 t}{U^2 \lambda} \ln^2 \left\{ 1 + \frac{U(W_0 - W_C)}{q_L} \right\} \\ &= 2 \left(\frac{k}{c}\right)^2 \frac{h}{H_W} \frac{q_L^2}{(W_0 - W_C) U^2} q_L t \ln^2 \left\{ 1 + \frac{U(W_0 - W_C)}{q_L} \right\} \end{aligned} \quad (39)$$

Equation (39) can be used in equation (19) for the drift to account for uplift. Other results also have to be updated accordingly. The approach outlined above needs to be benchmarked with numerical simulations.



5.3 First-passage and floodplain age distributions

500 The Lévy distribution (eq. 33) describes the time needed until the channel moves a particular distance away from its starting location. When integrated to infinity, the distribution has an infinite mean and variance. Nevertheless, under the assumption of constant or effective flow conditions, it could be used, for example, for assessing the risk of the destruction of a building near a river channel within a given timespan.

505 Lateral river dynamics determine the reworking of sediment in the floodplain, and, therefore, determine storage times and sediment ages (e.g., Bradley & Tucker, 2013). This has, for example, implications for chemical alteration of floodplain sediments, such as chemical weathering and organic carbon oxidation (e.g., Repasch et al., 2020; Torres et al., 2017). It has frequently been found residence time distributions are highly skewed, and that the mean residence time of sediment is much larger than their median residence time (e.g., Carretier et al., 2020; Pizzuto et al., 2017). Measurements of the distribution of floodplain ages have yielded a variety of contrasting behaviour (Pizzuto et al., 2017). The right-hand tail of the distribution of field data has been characterized both, by an exponential (e.g., Huffman et al., 2022; Lancaster & Casebeer, 2007) and by a power law function (e.g., Bradley & Tucker, 2013; Pizzuto et al., 2017), in the latter case with exponents ranging from about -0.7 to -1.5 (e.g., Everitt, 1968; Lancaster et al., 2010; Pizzuto et al., 2017; Skalak & Pizzuto, 2010). Pizzuto et al. (2017) used a random walk to model the stochastic downstream motion of sediment to predict power-law travel-time distributions with exponents that decrease with increasing length of the river system.

515 Bradley & Tucker (2013) suggested that the Lévy distribution is suitable to model the distribution of floodplain ages. Analogous to our result for the age distribution (eq. 34), the Lévy distribution features a power-law right-hand tail with a scaling exponent of -1.5 (eq. 33). However, it strongly underpredicted the likelihood of small ages as generated by Bradley & Tucker's (2013) numerical model. The Lévy distribution has been derived for the time of the first passage of a point a pre-selected distance from the origin (eq. 33), and this distance cannot be equal to zero in the assumptions of the derivation. It therefore is not the correct distribution for the times to return to the origin. We derived a probability distribution for the time to return to the origin (eq. 34). The right-hand tail of the residence time distribution (eq. 35) exhibits the same scaling of the right-hand tail of the Lévy distribution (eq. 33), a power law with an exponent of -1.5 (Fig. 6b). In fact, this scaling is valid for any symmetric random walk, and should be independent of the precise assumptions used to set up such a random walk. It implies that the return-time distribution has both an infinite mean and standard deviation when integrated to infinity, similar to the distribution of first passage. This result implies that the mean age measured for a sediment body within a channel belt does not converge to a fixed value, but depends on the time since the onset of fluvial activity, no matter how long ago this onset occurred. The result implies that statements on the age of sediment in floodplains, or their chemical alteration, always have to be made with respect to the total age of the floodplain. A long-term average at steady state is never achieved. Further, it implies that some fluvial deposits are likely to survive for long times, storing information about the floodplain evolution and



530 the history of river systems (cf. Carretier et al., 2020). The increase of the mean sediment residence time \overline{T}_R can be obtained by integrating the age distribution (eq. 34) multiplied with time, as in the integration for the mean. We can obtain the limit behaviour for old river systems by integrating over eq. (35)

$$\overline{T}_R(t) = \int_0^{T_A} \frac{\lambda}{\sqrt{2\pi}} \left(\frac{h}{H_W} t \right)^{-3/2} t dt = \sqrt{\frac{2}{\pi}} \left(\frac{H_W}{h} \right)^3 \frac{T_A}{\lambda}. \quad (40)$$

535 Here, T_A is the time since the formation of the channel belt. The mean residence time thus increases with the square root of time in this limit. In combination with eq. (35), eq. (40) can be used to estimate the age of a channel belt from sediment age data.

Our prediction of the -1.5-scaling exponent in the age distribution (eqs. 34, 35) does align with some, but not all of the
540 measurements reported in the literature (cf. Pizzuto et al., 2017). It is consistent with the data of Everitt (1966), Skalak & Pizzuto (2010), and Huffmann et al. (2022) that we digitised for the present study (Fig. 6c), but not with the datasets reported for example by Lancaster et al. (2010). Our model framework is strictly valid only for processes that can be modelled by a lateral random walk in an infinite domain. We expect that the -1.5-scaling applies to channels that are short enough such that sediment, once it is eroded, is not redeposited within the system, but evacuated downstream. Alternatively, it could apply for
545 dating methods where the date is reset after remobilization of sediment, for example optically stimulated luminescence (e.g., Madsen & Murray, 2009). Multiple episodes of deposition and erosion within the same system yields a power-law tail with an exponent that is dependent on the system size (Pizzuto et al., 2017). This exponent should, generally, be smaller than -1.5, because re-deposition will increase the relative fraction of old sediment. Even in short systems, the derived age distribution (eq. 34) cannot be expected to be universally applicable. We expect that channels confined in a narrow valley, or those in
550 which processes other than lateral channel migration can deposit, evacuate or mobilize sediment, show different scaling behaviour. For example, Cedar Creek and Golden Ridge Creek, both channels in confined valleys where debris flows regularly supply and mobilize sediment (Lancaster et al., 2010), exhibit age distributions with power-law scaling exponents of the order of -0.7. In narrowly confined settings, sediment deposition and erosion may not be adequately described by a random walk. Further, lateral sediment supply due to debris flows or hillslope processes may have a large effect on the age distribution.

555 **5.4 Parameter estimation and further tests**

Two of the parameters in the model need further scrutiny. First, the hydraulic and geometric controls on the lateral transport capacity q_L are not fully resolved. This parameter can, in principle, be investigated in experiments (e.g., Bufe et al., 2019; Wickert et al., 2013) and nature (e.g., Constantine et al., 2014; Greenberg & Ganti, 2024; Ielpi & Lapôtre, 2019). Bufe et al. (2019) presented a discussion and synthesis of the available evidence from experimental and natural channels, as well as a
560 dimensionless analysis of potential control parameters. We will not further discuss this parameter here. Second, the model



contains a single dimensionless scaling factor, k , which is the factor of proportionality of the rate of switches of direction of motion of the channel λ and the ratio of the lateral transport capacity q_L and the square of the flow depth h (eq. 2). This parameter sets the unconfined channel-belt width (eq. 4). Two strategies for measuring this parameter appear from our results. First, exploiting eq. (2) relies on direct measurements of the switching rate, as well as flow depth and q_L . The switching rate λ can also be measured from the age distribution of sediment (eq. 41). Second, the width of the channel belt can be related to flow depth and channel width using eq. (4). Both approaches seem more promising in an experimental setting than in nature, because the necessary parameters can be either controlled or measured directly. In the field, it may be possible to obtain suitable data, for example, from time series of orthophotos of river reaches (e.g., Nyberg et al., 2023; Greenberg & Ganti, 2024; Greenberg et al., 2024) in combination with gauging data. Testing for the consistency of both approaches would be a strong method to falsify or validate the model.

Camporeale et al. (2005) studied models of meandering rivers at increasing levels of hydraulic detail. They concluded that the steady state statistics of the meander belt are determined by only two parameters, regardless of the complexity of the model. These are a length scale D_0 [L] proportional to the ratio of flow depth and the friction coefficient of the open channel flow C_f

$$D_0 = \frac{h}{2C_f}, \quad (41)$$

and a time scale T_0 [T], given by

$$T_0 = \frac{D_0^2}{W_c U_f E}. \quad (42)$$

Here, U_f [LT^{-1}] is the mean streamwise flow speed and E [-] a dimensionless bank erodibility coefficient. Using their model considerations together with field observation, Camporeale et al. (2005) found that the meander belt width W_{MB} can be described by

$$W_{MB} = \alpha D_0 = \frac{\alpha h}{2C_f}. \quad (43)$$

Here, α [-] is a dimensionless proportionality coefficient with a value of 40 to 50. We can use eqs. (41) to (43) to make a tentative connection between our landscape-scale random walk model, and the reach-scale meandering models. First, we note both models suggest that channel-belt width is proportional to flow depth (see eq. 4). Comparing eqs. (4) and (43), we suggest that k_0 scales as

$$k_0 = \frac{c}{k} = \frac{\alpha}{2C_f}. \quad (44)$$



As such, we expect k to scale with the friction coefficient. Assuming $C_f = 0.05$ and $\alpha = 50$ (see Camporeale et al., 2005), we obtain $k = 0.0045$ and $k_0 = 500$. Second, we can assume that the governing time scale τ (eqs. 13, 14) is proportional to T_0 . Equating eqs. (14) and (42), and substituting eqs. (2), (41), and (43), we obtain

595

$$\frac{c}{\lambda} = \frac{ch^2}{kq_L} = \frac{\alpha h^2}{2C_f q_L} = \frac{D_0^2}{W_c U_f E} = \left(\frac{h}{2C_f} \right)^2 \frac{1}{W_c U_f E} \quad (45)$$

Equation (45) can be solved for q_L to give

$$q_L = 2\alpha C_f W_c U_f E. \quad (46)$$

600

We can obtain some of the parameter values from the data used in this study. From fits to the age distribution, we obtain $\lambda = 0.12 \text{ yr}^{-1}$ (Everitt, 1966), $\lambda = 0.55 \text{ yr}^{-1}$ (Skalak & Pizzuto, 2010), and $\lambda = 0.00097 \text{ yr}^{-1}$ (Huffmann et al., 2022). Note that we assumed an unconfined channel belt for determining λ , i.e., we set $H_w = h$. In case of confinement, the estimates change with the ratio of the flow depth and the height of the confining walls (eq. 35). The numbers for the mean rate of switching seem plausible, varying from biannual switches (Skalak & Pizzuto, 2010) to once in a thousand years (Huffmann et al., 2022). The estimates should be further refined with detailed case studies.

605

5.5 Beyond the evolution of single cross sections

In the model developed herein, we concentrated on a single cross section, making the assumption that each cross section evolves independently of those upstream and downstream. This assumption is unlikely to apply in a real river system. In particular, we can expect that a channel that locally moves laterally far from the channel position upstream and downstream is pulled back towards the center. That is, a channel within a particular cross section of the valley is less likely to further migrate laterally into the same direction if within the cross sections upstream and downstream the channel has not migrated as far, or is moving in the opposite direction. This effect can be included into the model by modulating the probability of switching direction λ within the cross section of interest depending on the position of its channel with respect to the entire river system or to the cross sections immediately upstream and downstream. We suggest that the behaviour can be modelled by an Ornstein-Uhlenbeck process (e.g., Uhlenbeck & Ornstein, 1930), similar to the Langevin equation (Langevin, 1908), which includes a term that increases the probability to move back towards the origin as a function of the distance from it. It is beyond the scope of the present contribution to develop such a model. We expect that the suggested approach will yield a Gaussian distribution of channel positions, with similar results to those derived herein, but additional dimensionless scaling factors in the variances.

615



620 **6. Conclusion**

We have described the temporal evolution of channel-belt width in the framework of a random walk. Our work provides a theoretical framework to interpret observational data. The predicted scaling exponent for the age distribution of floodplain sediments is consistent with observations. In the experimental data (Bufe et al., 2016a,b, 2019), average widening proceeds with the squareroot of time, as expected for the drift phase. Recent global datasets on channel belts derived by automatic
625 processing of remote sensing data (e.g., Greenberg & Ganti, 2024, Greenberg et al., 2024; Nyberg et al., 2023) provide opportunities for comprehensive testing of the model. We have provided a range of analytical results (Table 1) that allow easy comparison of theory and data. These can also be directly implemented into landscape evolution models without major numerical costs, allowing a more comprehensive and realistic depiction of landscape dynamics. Further, all model parameters have a direct physical interpretation, and there is a single free, dimensionless scaling parameter that needs to be informed by
630 data. As such, our approach can bridge across spatio-temporal scales and connect landscape-scale models with those operating on the process scale.



Symbols & Notation

<i>Symbol</i>	<i>Parameter</i>	<i>First appears in eq.</i>
α	Dimensionless proportionality coefficient with a value of 40 to 50 [-]	42
λ	Rate parameter of the Poisson process describing the switch in the direction of river motion [T ⁻¹]	2
τ	Governing timescale for the transient approach to a steady state [T]	12
a	Dimensionless constant approximately equal to 1.1135 [-]	36
b	Distance of an point of interest from the river channel at $t = 0$ [L]	33
c	dimensionless constant approximately equal to 2.2285 [-]	3
C_f	Open channel flow friction coefficient [-]	40
D_0	Characteristic length scale of meander belts [L]	40
E	Dimensionless bank erodibility coefficient [-]	41
h	Flow depth [L]	2
H_+	Height of the river bank in the direction of river motion [L]	1
H_W	Height of the walls confining the channel belt [L]	17
k	Dimensionless constant of order 10 ⁻² to 10 ⁻³ [-]	2
k_0	Dimensionless constant of order 10 ² , defined by c/k [-]	4
n	Number of stochastic events, generally used for the number of steps in the random walk [-]	6
m	Number of pairs of steps in the random walk, generally defined as $n/2$ [-]	
q_H	Rate of lateral sediment supply from hillslopes or valley walls per channel length [L ² T ⁻¹]	5
q_L	Lateral-transport capacity, i.e. the amount of sediment that the channel can move by lateral erosion per unit channel length per unit time [L ² T ⁻¹]	1
P	Fraction of time that a river spends at any of its channel belt margin [-]	9
$P_{confined}$	Fraction of time that a river spends at any of its channel belt margins for a confined belt [-]	15
S	Dimensionless envelope distance for the channel belt in the law of the iterated logarithm [-]	31
t	Time [T]	4
t^*	Dimensionless time [-]	31
Δt	Average switching timescale in the Poisson process [T]	6
T_0	Characteristic time scale of meander belts [T]	41
ΔT	The characteristic length of time the river moves on average in the same direction [T]	3
T_A	Time since the formation of the channel belt; age of the channel belt [T]	40
T_{FP}	First passage time, first point in time when the channel reaches at a point of interest located	33



	a distance b from the channel at $t = 0$ [T]	
T_R	Time needed to return to the origin for the first time [T]	34
\bar{T}_R	Mean residence time of sediment [T]	
T_{SS}	Time at which the steady state width is reached [T]	27
T_W	Waiting times between events in a Poisson process [T]	7
U	Uplift rate [$L T^{-1}$]	5
U_f	Mean streamwise flow speed [$L T^{-1}$]	41
v	Lateral speed of the river as it reaches valley-floor margins, i.e. wall toes [$L T^{-1}$]	15
V	Lateral migration speed, i.e. the speed of river migrating back and forth across the valley floor [$L T^{-1}$]	1
\bar{v}	Average lateral channel migration speed in a confined channel belt [$L T^{-1}$]	23
V_{Drift}	Average lateral speed of a channel belt with constant width during the drift phase [$L T^{-1}$]	29
VAR_{CCB}	Variance of a confined channel-belt width [L^2]	24
VAR_{UCB}	Variance of an unconfined channel-belt width [L^2]	19
W	Channel-belt width [L]	5
W_c	River channel width [L]	4
W_{Drift}	Width of channel belt in the drift phase [L]	19
W_{MB}	Width of a meander belt [L]	42
W_V	Valley floor width [L]	5
W_0	Unconfined channel-belt width [L]	4
Δx	Distance travelled by the channel before switching direction for the first time [L]	34
X	Envelope distance for the channel belt in the law of the iterated logarithm, dimensional version of S [L]	32
X_{Drift}	Average distance drifted in the drift phase [L]	26



635 **Data availability**

Raw data for the experimental datasets are stored on the SEAD repository of Bufe et al. (2016b) with the identifier <http://dx.doi.org/10.5967/M0CF9N3H>. Derived quantities have been compiled from Bufe et al. (2016a,b) and Bufe et al. (2019). Sediment age data were digitised from the respective publications. Scripts used to generate Figures 2-7 are available in the publication by McNab (2024) with identifier <https://doi.org/10.5281/zenodo.12806574>.

640

Competing interests

At least one of the (co-)authors is a member of the editorial board of Earth Surface Dynamics. The authors also have no other competing interests to declare.

645 **Author contributions**

JMT, AB and ST conceived this study. JMT designed and developed the theoretical approach and derived the equations with input of FM and AB, and wrote the paper. FM wrote the scripts for the numerical model and generated data figures. ST made illustrations. FM and AB developed and conducted the analysis of the experimental data. All authors contributed to data analysis, discussion, and writing.

650

Acknowledgments

Sophie Katzung implemented a first numerical realisation of the Poisson model and explored some of the implications of the random walk formulation during an internship. FM was supported by ERC Consolidator Grant #863490 GyroSCoPe to Taylor Schildgen.

655 **References**

- Allen, J. R. L. (1978). Studies in fluvial sedimentation: An exploratory quantitative model for the architecture of avulsion-controlled alluvial suites. *Sedimentary Geology*, 21(2), 129–147. [https://doi.org/10.1016/0037-0738\(78\)90002-7](https://doi.org/10.1016/0037-0738(78)90002-7), 1978.
- Anderson, M. P., Aiken, J. S., Webb, E. K., & Mickelson, D. M.: Sedimentology and hydrogeology of two braided stream deposits. *Sedimentary Geology*, 129(3-4), 187–199. [https://doi.org/10.1016/S0037-0738\(99\)00015-9](https://doi.org/10.1016/S0037-0738(99)00015-9), 1999.
- 660 Badoux, A., Andres, N., & Turowski, J. M.: Damage costs due to bedload transport processes in Switzerland, *Natural Hazards and Earth System Science*, 14, 279-294, <https://doi.org/10.5194/nhess-14-279-2014>, 2014.
- Baley, P. B.: The flood pulse advantage and the restoration of river-floodplain systems, *Regulated Rivers: Research & Management*, 6, 75-86, <https://doi.org/10.1002/rrr.3450060203>, 1991.
- Bertoldi, W., Zanoni, L., & Tubino, M. (2009). Planform dynamics of braided streams. *Earth Surface Processes and Landforms*, 34(4), 547–557. <https://doi.org/10.1002/esp.1755>
- 665



- Blum, M., Martin, J., Milliken, K., & Garvin, M.: Paleovalley systems: Insights from Quaternary analogs and experiments. *Earth-Science Reviews*, 116, 128–169. <https://doi.org/10.1016/j.earscirev.2012.09.003>, 2013.
- Bradley, D. N., & Tucker, G. E.: The storage time, age, and erosion hazard of laterally accreted sediment on the floodplain of a simulated meandering river, *Journal of Geophysical Research*, 118, 1308–1319, <https://doi.org/10.1002/jgrf.20083>, 2013.
- 670 Bridge, J. S.: Characterization of fluvial hydrocarbon reservoirs and aquifers: problems and solutions. *Latin American Journal of Sedimentology and Basin Analysis*, 8(2), 87–114, 2001.
- Bridge, J. S., & Leeder, M. R.: A simulation model of alluvial stratigraphy, *Sedimentology*, 26, 617–644, <https://doi.org/10.1111/j.1365-3091.1979.tb00935.x>, 1979.
- Bufe, A., Burbank, D. W., & Paola, C.: Fold erosion by an antecedent river, University of Michigan ARC Repository, 340
675 <http://dx.doi.org/10.5967/M0CF9N3H>, 2016b.
- Bufe, A., Paola, C., & Burbank, D. W.: Fluvial bevelling of topography controlled by lateral channel mobility and uplift rate, *Nature Geoscience*, 9(9), 706–710, <https://doi.org/10.1038/ngeo2773>, 2016a.
- Bufe, A., Turowski, J. M., Burbank, D. W., Paola, C., Wickert, A. D., & Tofelde, S.: Controls on the lateral channel-migration rate of braided channel systems in coarse non-cohesive sediment: *Earth Surface Processes and Landforms*, 44(14), 2823–
680 345 2836, <https://doi.org/10.1002/esp.4710>, 2019.
- Carretier, S., Guerit, L., Harries, R., Regard, V., Maffre, P., & Bonnet, S.: The distribution of sediment residence times at the foot of mountains and its implications for proxies recorded in sedimentary basins, *Earth and Planetary Science Letters*, 546, 116448, <https://doi.org/10.1016/j.epsl.2020.116448>, 2020.
- Constantine, J. A., Dunne, T., Ahmed, J., Legleiter, C., & Lazarus, E. D.: Sediment supply as a driver of river meandering and
685 floodplain evolution in the Amazon Basin. *Nature Geoscience*, 7(12), 899–903. <https://doi.org/10.1038/ngeo2282>, 2014.
- Egozi, R., & Ashmore, P.: Experimental analysis of braided channel pattern response to increased discharge. *Journal of Geophysical Research*, 114, F02012. <https://doi.org/10.1029/2008JF001099>, 2009.
- Everitt, B.L.: Use of the cottonwood in an investigation of the recent history of a flood plain, *Am. J. Sci.*, 266, 417–439, 1968.
- Fotherby, L. M.: Valley confinement as a factor of braided river pattern for the Platte River, *Geomorphology*, 103, 562–576,
690 <https://doi.org/10.1016/j.geomorph.2008.08.001>, 2009.
- Greenberg, E., & Ganti V.: The pace of global river meandering influenced by fluvial sediment supply, *Earth Planet. Sci. Lett.*, 634, 118674, <https://doi.org/10.1016/j.epsl.2024.118674>, 2024.
- Greenberg, E., Chadwick, A. J., Li, G. K., & Ganti V.: Quantifying channel mobility and floodplain reworking timescales across river planform morphologies, *Geophys. Res. Lett.*, 51, e2024GL108537, <https://doi.org/10.1029/2024GL108537>,
695 2024.
- Junk, W. J., Bayley, P. B., & Sparks, R. E.: The flood pulse concept in river-floodplain systems, p. 110–127 in D. P. Dodge (Ed.), *Proceedings of the International Large River Symposium*. Can. Spec. Publ. Fish. Aquat. Sci. 106, 1989.
- Hajek, E. A., & Straub, K. M.: Autogenic sedimentation in clastic stratigraphy. *Annual Review of Earth and Planetary Sciences*, 45(1), 681–709. <https://doi.org/10.1146/annurev-earth-063016-015935>, 2017.



- 700 Hancock, G. S., & Anderson, R. S.: Numerical modeling of fluvial strath-terrace formation in response to oscillating climate. *Bulletin of the Geological Society of America*, 114(9), 1131–1142. [https://doi.org/10.1130/0016-3507606\(2002\)114<1131:NMOFST>2.0.CO;2](https://doi.org/10.1130/0016-3507606(2002)114<1131:NMOFST>2.0.CO;2), 2002.
- Howard, A. D.: Modelling Channel Evolution and Floodplain Morphology, In M. G. Anderson, D. E. Walling, & P. E. Bates (Eds.), *Floodplain processes* (pp. 15–62). Chichester: John Wiley and Sons, Ltd., 1996.
- 705 Huffman, M. E., Pizzuto, J. E., Trampush, S. M., Moody, J. A., Schook, D. M., Gray, H. J., & Shannon, A. M.: Floodplain sediment storage timescales of the laterally confined meandering Powder River, USA, *J. Geophys. Res.*, 127, e2021JF006313, <https://doi.org/10.1029/2021JF006313>, 2022.
- Ielpi, A., & Lapôtre, M. G. A.: A tenfold slowdown in river meander migration driven by plant life, *Nature Geoscience*, 13, 82–86, <https://doi.org/10.1038/s41561-019-0491-7>, 2019.
- 710 Jonell, T. N., Owen, L. A., Carter, A., Schwenniger, J.-L., & Clift, P. D.: Quantifying episodic erosion and transient storage on the western margin of the Tibetan Plateau, upper Indus River. *Quaternary Research*, 89, 281–306, <https://dx.doi.org/10.1017/qua.2017.92>, 2018.
- Kolmogoroff, A.: Über das Gesetz des iterierten Logarithmus, *Mathematische Annalen*, 101, 126–135, 1929.
- Lancaster, S. T., & Casebeer, N. E.: Sediment storage and evacuation in headwater valleys at the transition between debris-
715 flow and fluvial processes, *Geology*, 35(11), 1027–1030, <https://dx.doi.org/10.1130/G239365A.1>, 2007.
- Lancaster, S. T., Underwood, E. F., & Frueh, W. T.: Sediment reservoirs at mountain stream confluences: dynamics and effects of tributaries dominated by debris-flow and fluvial processes, *Geol. Soc. Am. Bull.*, 122, 1775–1786, <https://dx.doi.org/10.1130/B30175.1>, 2010.
- Langevin, M. P.: On the theory of Brownian motion, *C. R. Acad. Sci. (Paris)* 146, 530–533, 1908.
- 720 Lawler, G. F., & Limic, V.: *Random Walk: A modern introduction*, Cambridge University Press, ISBN 9780511750854, <https://doi.org/10.1017/CBO9780511750854>, 2010.
- Limaye, A. B. S.: How do braided rivers grow channel belts? *Journal of Geophysical Research: Earth Surface*, 125, 1–24. <https://doi.org/10.1029/2020JF005570>, 2020.
- Maddy, D., Bridgland, D., & Westaway, R.: Uplift-driven valley incision and climate-controlled river terrace development in
725 the Thames Valley, UK. *Quaternary International*, 79(1), 23–36. [https://doi.org/10.1016/s1040-6182\(00\)00120-8](https://doi.org/10.1016/s1040-6182(00)00120-8), 2001.
- Madsen, A. T., & Murray, A. S.: Optically stimulated luminescence dating of young sediments: A review, *Geomorphology*, 109, 3–16. <https://doi.org/10.1016/j.geomorph.2008.08.020>, 2009.
- Malatesta, L. C., Prancevic, J. P., & Avouac, J. P.: Autogenic entrenchment patterns and terraces due to coupling with lateral erosion in incising alluvial channels. *Journal of Geophysical Research: Earth Surface*, 122, 335–355. <https://doi.org/10.1002/2015JF003797>, 2017.
- 730 Martin, J., Cantelli, A., Paola, C., Blum, M., & Wolinsky, M.: Quantitative modeling of the evolution and geometry of incised valleys. *Journal of Sedimentary Research*, 81(1), 64–79. <https://doi.org/10.2110/jsr.2011.5>, 2011.



- May, C., Roering, J., Eaton, L. S., & Burnett, K. M.: Controls on valley width in mountainous landscapes: The role of 360
landsliding and implications for salmonid habitat. *Geology*, 41(4), 503–506. <https://doi.org/10.1130/G33979.1>, 2013.
- 735 McNab, F.: Supplement to: "Width evolution of channel belts as a random walk" by Turowski et al., Version 1, Zenodo,
<https://doi.org/10.5281/zenodo.12806574>, 2024.
- Meitzen, K. M., Kupfer, J. A., & Gao, P.: Modeling hydrologic connectivity and virtual fish movement across a large
Southeastern floodplain, USA, *Aquatic Sciences*, 80(5), <https://doi.org/10.1007/s00027-017-0555-y>, 2018.
- Miller, A. J.: Valley morphology and boundary conditions influencing spatial patterns of flood flow. In: Costa, J. E., Miller,
740 A. J., Potter, K. W., Wilcock, P. R. (Eds.), *Natural and Anthropomorphic Influences in Fluvial Geomorphology*.
Geophysical Monograph, 89. American Geophysical Union, Washington, DC, 57–81,
<https://doi.org/10.1029/GM089p0057>, 1995.
- Naiman, R. J., Bechtold, J. S., Beechie, T. J., Latterell, J. J., & Van Pelt, R.: A process-based view of floodplain forest patterns
in coastal river valleys of the Pacific Northwest, *Ecosystems*, 13, 1-31, <https://doi.org/10.1007/s10021-009-9298-5>, 2010.
- 745 Nyberg, B., Henstra, G., Gawthorpe, R. L., Ravnås, R., & Ahokas, J.: Global scale analysis on the extent of river channel belts,
Nature Communications, 14, 2163, <https://doi.org/10.1038/s41467-023-37852-8>, 2023.
- Pizzuto, J., Keeler, J., Skalak, K., & Karwan, D.: Storage filters upland suspended sediment signals delivered from watersheds,
Geology, 45(2), 151-154, <https://doi.org/10.1130/G38170.1>, 2017.
- Redner, S.: *A Guide to First Passage Time Processes*, 328 pp., Cambridge Univ. Press, New York. 2001.
- 750 Repasch, M., Wittmann, H., Scheingross, J. S., Sachse, D., Szupiany, R., Orfeo, O., Fuchs, M., & Hovius, N.: Sediment transit
time and floodplain storage dynamics in alluvial rivers revealed by meteoric ¹⁰Be, *Journal of Geophysical Research: Earth
Surface*, 125, e2019JF005419, <https://doi.org/10.1029/2019JF005419>, 2020.
- Repasch, M., Scheingross, J. S., Hovius, N., Lupker, M., Wittmann, H., Haghipour, N., Gröcke, D. R., Eglinton T. I., and
Sachse, D.: Fluvial organic carbon cycling regulated by sediment transit time and mineral protection, *Nat. Geosci.*, 14,
755 842–848, <https://doi.org/10.1038/s41561-021-00845-7>, 2021.
- Schumm, S. A., & Lichty, R. W.: Flood-plain construction along Cimarron River, in southwestern Kansas, *Geol. Surv. Prof.*
Pap. 352-DUS Gov. Printing Office, Washington, 1963. 365
- Skalak, K., & Pizzuto, J.: The distribution and residence time of suspended sediment stored within the channel margins of a
gravel-bed bedrock river, *Earth Surface Processes and Landforms*, 35, 435-446, <https://doi.org/10.1002/esp.1926>, 2010.
- 760 Tofelde, S., Bernhardt, A., Guerit, L., & Romans, B. W.: Times associated with source-to-sink propagation of environmental
signals during landscape transience, *Front. Earth Sci.*, 9, 628315, <https://doi.org/10.3389/feart.2021.628315>, 2021.
- Tofelde, S., Bufe, A., & Turowski, J. M.: Hillslope sediment supply limits alluvial valley width, *AGU Advances*, 3,
e2021AV000641. <https://doi.org/10.1029/2021AV000641>, 2022.
- Torres, M. A., Limaye, A. B., Lamb, M. P., West, A. J., & Fischer, W. W.: Model prediction of long-lived storage of organic
765 carbon in river deposits, *Earth Surface Dynamics*, 5, 711-730, <https://doi.org/10.5194/esurf-5-711-2017>, 2017.



- Turowski, J. M., Bufe, A., & Tofelde, S.: A physics-based model for fluvial valley width, *Earth Surface Dynamics*, 12, 493-514, <https://doi.org/10.5194/esurf-12-493-2024>, 2024.
- Uhlenbeck, G. E., & Ornstein, L. S.: On the theory of the Brownian motion, *Phys. Rev.* 36, 823-841, <https://doi.org/10.1103/PhysRev.36.823>, 1930.
- 770 van de Lageweg, W. I., van Dijk, W. M., & Kleinhans, M. G. (2013). Channel belt architecture formed by a meandering river. *Sedimentology*, 60(3), 840–859. <https://doi.org/10.1111/j.1365-3091.2012.01365.x>
- Wickert, A. D., Martin, J. M., Tal, M., Kim, W., Sheets, B., & Paola, C.: River channel lateral mobility: Metrics, time scales, and controls. *Journal of Geophysical Research: Earth Surface*, 118, 396–412. <https://doi.org/10.1029/2012JF002386>, 2013.